Dissipative Particle Dynamics Simulations in the Grand Canonical Ensemble: Applications to Polymer Brushes

Florent Goujon,[a] Patrice Malfreyt,*[a] and Dominic J. Tildesley[b]

We have used the dissipative particle dynamics (DPD) method in the grand canonical ensemble to study the compression of grafted polymer brushes in good solvent conditions. The force–distance profiles calculated from DPD simulations in the grand canonical ensemble are in very good agreement with the self-consistent field (SCF) theoretical models and with experimental results for two polystyrene brush layers grafted onto mica surfaces in toluene.

Introduction

Polymers grafted onto surfaces have applications in many important technical problems: wetting, adhesion, colloid stabilization and biocompatibility. At high surface coverages in good solvent conditions, the polymer chains are strongly stretched in the direction perpendicular to the grafted surface. The structure formed is called a polymer brush and results from a balance between the entropic elastic energy of the chain, the monomer–monomer interactions and the affinity for the solvent. When two brush layers are brought into contact, two new phenomena occur: interpenetration between the opposing brush layers and changes in the brush properties as a result of compression. There have been a significant number of experimental and theoretical studies on the properties of polymer brushes. Much of the computer simulation work on polymer brush systems has been carried out using molecular methods.

The fastest motions in a polymer system are the chemical bond stretching vibrations with times of the order of 10^{-14} s, whereas the relaxation time of the whole chain may exceed 1 ms. Moreover, numerous interesting polymer properties are observed at times of microseconds and beyond. A polymer chain exhibits structure from the scale of a chemical bond to the coil radius with collective phenomena on the length scale of microns. Simulations of polymer systems using a molecular description require solving the equations of motions on a timescale of 10^{-15} s and a length scale of Ångstroms. Atomistic simulation cannot reach the required length and timescales to study most polymer phenomena. One way to overcome these limitations is to use a coarse-grained description.

In this case we use a mesoscopic simulation technique, dissipative particle dynamics (DPD), to study the equilibrium properties of grafted polymer brushes in athermal solvent conditions.[1] The structural properties of polymer chains have been calculated as a function of the grafting density and the polymer chain length. In a recent study,[2] we reported the response of a grafted polymer to flow by using the sliding periodic boundary technique. The width of the layer, the friction coefficient and the structuring of the layer were calculated as a function of the shear rate and the quality of the solvent. Both of these studies were performed using a fixed separation between the surfaces. We have also established that the DPD method can reproduce the features of the equilibrium polymer brush behaviour and the rheological properties of polymer brushes. Herein, we plan to study the equilibrium polymer brushes as a function of the separation between the grafting surfaces.

The equilibrium conformations and force–distance profiles of compressed polymer brushes have been the subject of theoretical,[3–7] molecular simulation[8, 9] and experimental studies.[10–12] Compression in the simulation can be studied by three methods: keeping the total number of particles constant; keeping the density constant; or keeping the chemical potential of the solvent constant. Keeping the chemical potential constant models the situation in which the fluid between the surfaces is in equilibrium with a reservoir at the same temperature and chemical potential. This mimics the surface force apparatus where the compressions are measured experimentally.

Herein, we give a basic description of DPD simulations in the grand canonical ensemble with the appropriate transition probabilities. We check the method by simulating the excess pressure and excess chemical potential for the pure DPD fluid. We extend this study to grafted polymer brushes by comparing the calculated force–distance profiles with those deduced from theoretical models and experiments.

[a] *Dr. F. Goujon, Dr. P. Malfreyt*
Laboratoire de Thermodynamique des Solutions et des Polymères
UMR CNRS 6003, Université Blaise Pascal, 63177 Aubière Cedex (France)
Fax: (+33) 4-73-40-71-85
E-mail: patrice.malfreyt@univ-bpclermont.fr

[b] *Prof. D. J. Tildesley*
Unilever Research Port Sunlight, Bebington
Wirral (UK) CH63 3JW (United Kingdom)

 DOI: 10.1002/cphc.200300901

Results and Discussion

Dissipative Particle Dynamics Fluid

Before studying polymer brush systems, we performed canonical (*NVT*) simulations of a pure DPD fluid containing 5000 particles with periodic conditions applied in the three directions for ρ varying from 2.0 to 9.0. We took two values of the repulsive parameter ($a = a_{ij} = 30;60$). We computed the excess pressure using the virial theorem as a function of the density. We report these values in Figure 1. We thus find the same analytical

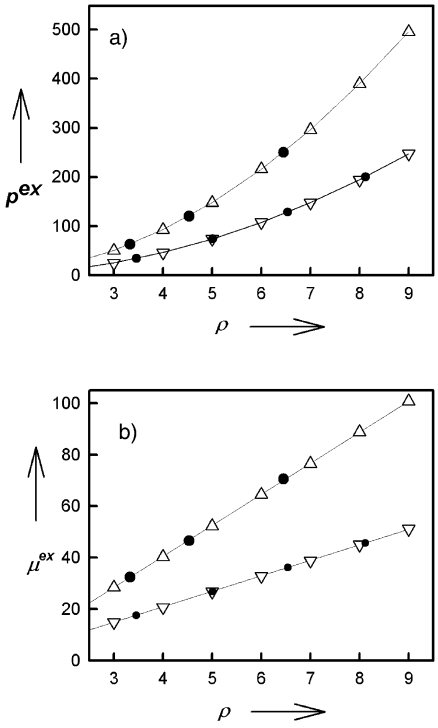

Figure 1. *a) Excess pressure and b) excess chemical potential calculated from pure DPD fluid simulations as a function of the density; the points calculated with* a = *60 (△) and* a = *30 (▽) result from* NVT *simulations, whereas the points (●) are from DPD simulations in the constant-*μVT *ensemble. The full curves represent the fits* $\alpha a \rho^2$ *and* $2\alpha a \rho$ *for the excess pressure and the excess chemical potential, respectively.*

shape for the equation of state for the excess pressure ($p^{ex} = \alpha a \rho^2$) as that obtained by Groot and Warren.[13] From the definition of the chemical potential and pressure as derivatives of the Helmholtz free energy, Equations (1)

$$\mu^{ex} = \left(\frac{\partial F}{\partial N}\right)_{V,T}, \; p^{ex} = -\left(\frac{\partial F}{\partial V}\right)_{T,N} \quad (1)$$

we find Equation (2) for the DPD fluid.

$$\frac{\partial \mu^{ex}}{\partial \rho} = 2\alpha a \quad (2)$$

In the *NVT* simulations of the pure DPD fluid, the simulation box in the *z* direction was divided into slabs of width $\Delta z = 0.2$. Rectangular plane grids of uniformly distributed test particles were inserted at different *z* positions 0.2 apart. The dimensions of the grids depended on the box size. For each particle, $\exp(-\Delta U^{test}/kT)$ was calculated and averaged for each plane separately, to obtain a value of the configurational chemical potential at a given *z*. For this homogenous DPD fluid, the average of the configurational chemical potential along the *z* direction gave a mean value which could be directly compared to the sum of excess chemical potential μ^{ex} and $kT \ln\rho$. The maximum deviation between these two calculations was found to be 0.2 %. We show the excess chemical potential as a function of the density (Figure 1). We find that the slope of this linear fit for the excess chemical potential is equal to $2\alpha a$, where $\alpha = 0.101 \pm 0.001$. This value is in perfect agreement with that previously calculated for the excess pressure equation of state.[13] This test establishes that the method of calculating the configurational chemical potential in a particular direction is reliable and accurate. To complete this test and to check the DPD algorithm in a constant-μVT ensemble, we performed different simulations at a given configurational chemical potential. At the end of the simulations, we again computed both the configurational chemical potential and the excess pressure from the saved configurations. We report these points in Figure 1. The excess chemical potential and the configurational chemical potential are given in Table 1 with the corresponding fixed chemical potential and the excess pressure. There is excellent agreement between the fixed chemical potential and that calculated over the saved configurations. The maximum deviation observed is 1 %. We also checked that the densities and excess pressures calculated from our simulations in the grand canonical ensemble obey the equation of state for the excess pressure. This additional test shows the validity of our DPD algorithm in this ensemble.

Table 1. *DPD simulations of pure DPD fluid in the constant-*μVT *ensemble using two values of the repulsive parameter* a. μ_{input} *is the input configurational chemical potential,* $\langle\rho\rangle$ *is the average density number,* p^{ex} *is the excess pressure calculated from the virial route,* $\langle\mu^{conf}\rangle_z$ *is the average configurational chemical potential calculated over the saved configurations and throughout the* z *direction and* μ^{ex} *is the excess chemical potential calculated from the standard Widom insertion method,* $\langle\mu^{conf}\rangle_V$ *is then defined as* $\mu^{ex} + kT\ln\rho$. *The number* 128.5_{11} *means* 128.5 ± 1.1.

μ_{input}	$\langle\rho\rangle$	p^{ex}	$\langle\mu^{conf}\rangle_z$	$\langle\mu^{ex}\rangle$	$\langle\mu^{conf}\rangle_V$
		Repulsive parameter $a = 30$			
20.0	3.46_1	34.0_4	20.0_1	17.5	20.0
30.0	5.01_1	73.81_7	29.9_1	26.7	29.9
40.0	6.54_1	128.5_{11}	39.7_2	36.1	39.8
50.0	8.12_1	200.3_{10}	49.7_2	45.7	49.9
		Repulsive parameter $a = 60$			
20.0	2.13_1	23.3_2	19.8_1	18.3	19.8
35.0	3.33_1	62.8_4	34.8_1	32.4	34.8
50.0	4.53_1	120.1_6	49.6_1	46.6	49.6
75.0	6.45_1	250.2_4	73.8_2	70.6	74.3

Polymer Brushes

The model used to describe the polymer brush system is composed of polymer chains, solvent particles and two planar

walls. The periodic boundary conditions are applied in the *x* and *y* directions; in the *z* direction the particles are confined by two walls. The polymer chains are tethered to the boundary walls to form two polymer brushes, one on the top and the other on the bottom of the box (Figure 2). The model consists of 108 grafted

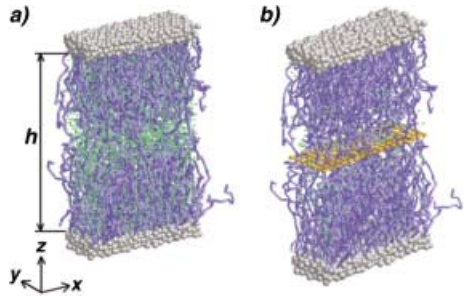

Figure 2. *a) Typical configuration for the polymer brush system studied here in good solvent conditions at* kT = *2.0;* h *is the distance separating the two surfaces. The polymer chains are represented using sticks and the green particles represent solvent particles. The grey particles represent wall particles that are uncovered. b) Similar configuration with a grid of ghost particles inserted at a* z *position.*

homopolymer chains attached to each wall and containing 20 polymer beads. Each wall contains 972 particles arranged in three hexagonally close packed layers. 108 particles of the layer nearest to the fluid were replaced by the first bead of the polymer chains. This resulted in a 33% grafting density. The number of solvent particles was 8393 and 222 for the weakest and highest compressions, respectively. The cell dimensions were: $L_x = 16.659$, $L_y = 6.412$ and L_z varied from 9.5 to 28.5. The simulations were performed in athermal solvent conditions when the repulsive force parameter was set to 60 for all the interactions. When the polymer–solvent interaction was lowered to 40, we simulated good solvent conditions. We defined h as the distance between the two grafting surfaces and h_0 as the distance separating the two surfaces at which the overlap between the two opposing brush layers vanished. $h_0/2$ is close to the height of an unperturbed brush or the maximum extent of a single brush. When the ratio h/h_0 was smaller than 1, the brushes came into overlap and they are described as compressed brushes. The system at which the distance between the surfaces is equal to h_0 is considered as the reference system. Our results will be compared with the experimental data obtained by Taunton and others[11] for two grafted polystyrene brush layers in toluene (a good solvent). To make our simulations closer to the experiments, we performed them in good solvent conditions with the repulsive parameter between polymer and solvent particles fixed at 40.

Equilibrium Thermodynamics

We have developed a simulation method, DPD in the grand canonical ensemble, to calculate the force–distance profiles between two grafting surfaces. In this technique, the number of solvent particles fluctuates during the simulations. Initially, we checked the thermal and mechanical equilibrium of this method. The thermal equilibrium was ensured using the calculation of the temperature profile of each component along the *z* direction perpendicular to the surfaces. The average temperature profile, $T_{zz}(z)$ is defined by Equation (3)

$$kT_{zz}(z) = \left\langle \frac{\sum_{i=1}^{N} H(z_i) m_i (\mathbf{v_i})_z \cdot (\mathbf{v_i})_z}{\sum_{i=1}^{N} H(z_i)} \right\rangle \quad (3)$$

where $H(z)$ is given by Equation (4)

$$H(z_i) = \begin{cases} 1 \text{ if } z - \Delta z/2 < z_i < z + \Delta z/2 \\ 0 \text{ otherwise} \end{cases} \quad (4)$$

where $\langle \ldots \rangle$ denotes an ensemble time average. $(\mathbf{v_i})_z$ is the *z* component of the velocity of particle *i* and m_i is the particle mass taken as unity. The simulation box along the *z* direction is divided into bins, each of which has a volume equal to $L_x L_y \Delta z$, where Δz is the width in the *z* direction of each bin ($\Delta z = 0.2$). Figure 3a shows that the T_{zz} component is uniform throughout the simulation box and equal to the input temperature defined by $kT = 2$, whatever the compression ratio. The profiles for the other components are similar. It also means that the perturbations (addition or destruction of solvent particles) do not prevent the system from relaxing towards its thermal equilibrium.

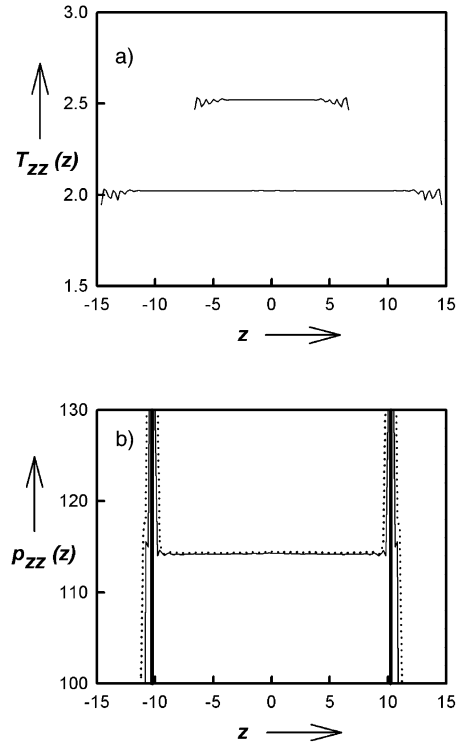

Figure 3. *a)* $T_{zz}(z)$ *component temperature profile calculated for the simulations in the constant-*μVT *ensemble for two different compression ratios. The temperature profile of the most compressed system has been displaced by 0.5 temperature units for clarity. b) The solid curve represents the normal component of the pressure tensor profile calculated using the IK definition[14, 15] for the simulations in the constant-*μVT *ensemble at a compression rate* ($h/h_0 = 0.77$) *whereas the dotted line represents the profile of the same component resulting from the MOP method.[16, 17] The bold lines give the positions for the two surfaces.*

For the pressure tensor calculation, we employed the Irving–Kirkwood[14, 15] definition (IK method). The normal pressure tensor is expressed by Equation (5)

$$p_{zz}(z) = \frac{1}{V}\left\langle \sum_{i=1}^{N} m_i(\mathbf{v_i})_z(\mathbf{v_i})_z \right\rangle + \frac{1}{A}\left\langle \sum_i \sum_{i<j} (\mathbf{z_{ij}})(\mathbf{F_{ij}})_z \frac{1}{|z_{ij}|}\theta\left(\frac{z-z_i}{z_{ij}}\right)\theta\left(\frac{z_j-z}{z_{ij}}\right) \right\rangle \quad (5)$$

where V is the volume of the basic bin and $A = L_x L_y$ is the surface area. $\theta\left(\frac{z-z_i}{z_{ij}}\right)$ is the unit step function which is equal to 1 when $\left(\frac{z-z_i}{z_{ij}}\right) > 0$ and zero otherwise. The distance z_{ij} between two particles i and j is divided into slabs of width $\Delta z = 0.2$ and the chains i and j contribute to the pressure tensor in a particular slab if the line joining i and j crosses, starts or finishes in the slab. The contribution from $i-j$ interaction is distributed uniformly along the line joining the particles i and j.

We also used an alternative definition of p based upon the method of planes (MOP)[16, 17] [Equation (6)].

$$p_{zz}(z) = \frac{1}{A}\left\langle \sum_{i=1}^{N} \frac{m_i(\mathbf{v_i})_z}{\delta t} \right\rangle + \frac{1}{A}\sum_i \sum_{i<j} (\mathbf{F_{ij}})_z [\theta(z_i - z)\theta(z - z_j) - \theta(z_j - z)\theta(z - z_i)] \quad (6)$$

In the method of planes, the kinetic part is calculated from the momentum flux.[18] If z_i and z_j are both either smaller or larger than z, the contribution to the pressure tensor is zero. If $z_i < z$ and $z_j > z$ then the first product of the Heaviside functions is zero and the second is unity. If $z_i > z$ and $z_j < z$ then the second is zero and the first is unity. In the method of planes, the pressure is computed across each plane and z corresponds to the position of the plane along the z direction whereas using the IK definition, z refers to the position of the kth volume element ($L_x \times L_y \times \Delta z$). The normal pressure components profiles (Figure 3b) are constant throughout the z direction for the two definitions used. Except for oscillations due to the tethered particles in the walls, the profiles are independent of z and thus allow a reliable calculation of the average normal component of the pressure tensor across the pore. The deviations between the local normal pressures resulting from the two definitions differ by less than 1% inside the pore. Figure 3b also shows the mechanical stability of our systems. We also checked the surface tension between the grafted polymer chains and the solvent particles. In good solvent conditions, it was close to zero, for all the compression ratios studied here.

For simulations of polymer brushes in good solvent conditions, the solvent density profile was not uniform along the direction perpendicular to the surfaces (Figure 4). The calculation of the configurational potential in the polymer brushes in good solvent conditions was carried out using the same Widom method used in the pure DPD fluid simulations. One hundred and nineteen test particles uniformly distributed in a rectangular plane grid (17×7) were inserted at different z positions 0.2 apart. Figure 4 shows the profiles of the solvent density and the configurational potential. We see that the local configurational chemical potential is independent of z even in the case of nonuniform density number. The fact that $\mu^{conf}(z)$ was constant across the simulation box allowed us to extract a unique value of the activity $\langle Z \rangle_z$ directly comparable to the fixed activity in the constant-μVT ensemble (see Equations (18) and (19) in the Computational Methods section). Using adapted algorithms, we have demonstrated that the polymer brush system in the constant-μVT ensemble is in thermal, mechanical and chemical equilibrium.

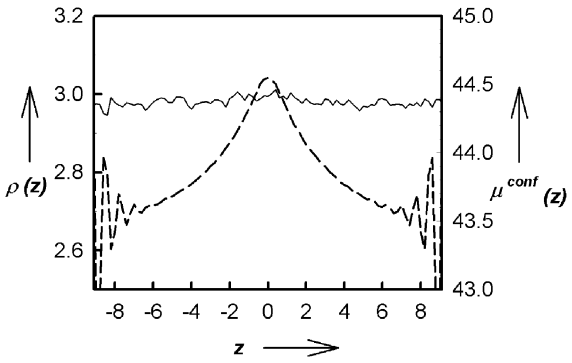

Figure 4. Solvent density (- - - -) and configurational chemical potential (——) profiles resulting from simulations for a compression ratio ($h/h_0 = 0.80$) in the constant-μVT ensemble.

Force–Distance Profiles

In studying compression, we compared the three different methods by keeping N, ρ or μ constant during the simulations. The calculated configurational chemical potentials are shown in Figure 5 as a function of the ratio (h/h_0) for the three approaches.

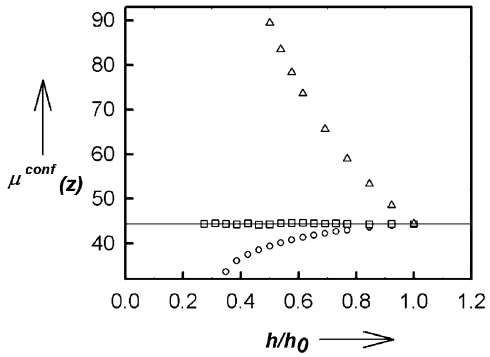

Figure 5. Calculated configurational chemical potential for the three methodologies: constant N (△), constant μ (□), constant ρ (○). The solid curve represents the configurational chemical potential calculated in the reference system.

Figure 5 shows that the simulations carried out with the total number of particles fixed gave a significant increase in the configurational chemical potential on compression. For ($h/h_0 = 0.5$), the configurational chemical potential is two times higher

than that calculated in the reference system. This means that it is very difficult to relate the experiments where the solvent is open to the bulk reservoir to simulations at constant *N*. We observe that the simulations at constant ρ are closer to those at constant μ, except at high compressions. We emphasise that most molecular simulations of polymer brush systems have been performed by keeping the solvent density constant at different compressions. We also checked that the calculated configurational chemical potential values in the constant-μVT ensemble matched those calculated in the reference system for all the compression ratios used here. Figure 6 shows the force–

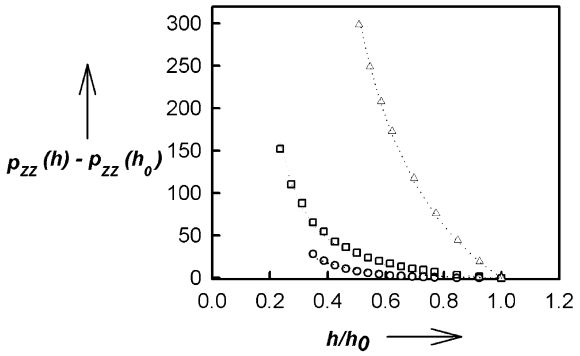

Figure 6. *Force–distance profiles between the two grafting surfaces calculated from the three methods: constant* N (△), *constant* μ (□), *constant* ρ (○).

distance profiles at different separations for the three methods. At each separation *h*, the average force per unit area *f*(*h*) between the two surfaces was calculated by subtracting the average normal pressure at $h = h_0$ from the average normal pressure at *h*. The forces are always repulsive. It also shows that the magnitude of the forces inside the pore depends on the methodology used and more precisely on the number of solvent particles present. We observed that the brush layers resulting from simulations with constant *N* were more resistant to compression than those calculated at constant μ and ρ. When $h/h_0 = 0.5$, the magnitude of the force was ten times higher in simulations with constant *N* than that in constant μ. With decreasing separation of the brushes, the increase in collisions is due to the higher monomer density number and implies an increase in the osmotic pressure in the brush which acts to swell the compressed brush, thus leading to an increase in the normal pressure. This increase in the magnitude of the forces is related to the number of solvent particles.

A scaling model of polymer chains adsorbed onto a surface by one end in good solvent conditions has been proposed by Alexander[3] and further extended by de Gennes[5] to the case of compressed polymer brushes to give an analytical expression of the force per unit area $f_1(h)$ as a function of *h*, Equation (7).

$$f_1(h) \approx \left[\left(\frac{h_0}{h}\right)^{\frac{9}{4}} - \left(\frac{h}{h_0}\right)^{\frac{3}{4}}\right] \tag{7}$$

The first term in Equation (7) comes from the osmotic pressure and is predominant at strong compressions. The second term describes the elastic term of the polymer chains. From the self-consistent field (SCF) method of Milner, Witten and Cates,[6] and after derivation of the free energy per unit area with respect to *h*, we obtained two expressions, Equations (8) and (9), of the force per unit area, differing in the form of the brush density profile. The first expression $f_2(h)$ predicts a very similar force law to the Alexander–de Gennes equation. The $f_1(h)$ and $f_2(h)$ force laws both suppose a flat brush profile, whereas the third expression, $f_3(h)$, considers the brush profile as parabolic.

$$f_2(h) \approx \left[\left(\frac{h_0}{h}\right)^{2} - \left(\frac{h}{h_0}\right)\right] \tag{8}$$

$$f_3(h) \approx \left[\frac{1}{2}\left(\frac{h_0}{h}\right)^{2} - \left(\frac{h}{h_0}\right) + \frac{1}{2}\left(\frac{h}{h_0}\right)^{4}\right] \tag{9}$$

These models assume a very little interpenetration between the two opposed brush layers and experiments do not provide an answer about this microscopic property. We have also calculated the interpenetration coefficient using the formula proposed by Murat and Grest[8] and found that it is not ever negligible, particularly at strong compressions. The interpenetration coefficient increases with decreasing surface separation, reaching a maximum value of 0.15 at the highest compression. Figure 7 a shows the semilogarithmic plot of the force–distance profiles as a function of the surface separation for the two methodologies considered. We have normalized the force–

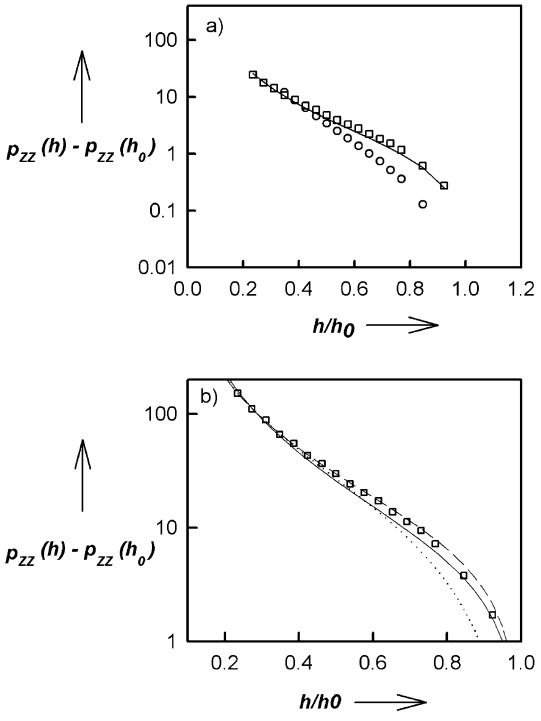

Figure 7. *a) Semilog plot of the force–distance profiles calculated from the simulations (□, constant* μ*) and (○, constant* ρ*). The solid curves represent the calculated profile with Alexander–de Gennes model, Equation (7). b) Semilog plot of the force–distance profile calculated in the constant-*μVT *ensemble (□). The solid curve represents the profile calculated from the Alexander–de Gennes model, whereas the dashed [Equation (8)] and dotted [Equation (9)] lines are based on the Milner–Witten–Cates model. The simulation results have been normalized to allow an overlap with the data calculated both with Alexander–de Gennes and Milner–Witten–Cates models.*

distance profiles in order to compare only the shape of these curves and fit them with the Alexander – de Gennes equation. We find a very good agreement between the simulations performed in the grand canonical ensemble and the Alexander – de Gennes model. To see this more clearly, we plotted the variation of the normal pressures calculated in the constant-μVT ensemble as function of the surface separation. The fitted curves using Equations (7), (8) and (9) are included for comparison (Figure 7 b). We checked that our results were well-predicted by the Alexander – de Gennes model. A very close agreement was also found with the model of Milner, Witten and Cates, assuming a flat monomer density profile, Equation (8). The fitting curve calculated using $f_3(h)$ with a parabolic polymer profile diverged from our results at weak compression and became closer to the $f_1(h)$ and $f_2(h)$ functions at strong compressions. As the compression became stronger, the third term in Equation (9) vanished and the three force laws have similar shapes. Figure 8

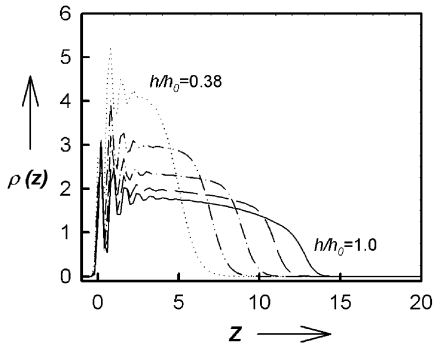

Figure 8. *Monomer density profiles of a brush layer calculated for five compression ratios* $h/h_0 = 1.0$*, solid curve;* $h/h_0 = 0.85$*, dashed curve;* $h/h_0 = 0.70$*, dash-dot curve;* $h/h_0 = 0.54$*, dash-dot-dot curve;* $h/h_0 = 0.38$*, dotted curve*

shows the monomer density profiles at various surface separations. These plots show that the profiles resemble a step function at weak compression and evolve towards a parabolic profile at higher compressions. This result explains why the fit with a model assuming a parabolic function is less good at weak compression. In order to make our simulations closer to the experiments of Taunton and others, we plotted the interaction energy per unit area $E(h)$, defined as the integral of the force per unit area $f(h)$ between h_0 and h. The experimental and calculated points are displayed in Figure 9. The results from experiments have been vertically shifted to lie on the simulated points for a direct comparison of their shapes. We observe good agreement between the interaction energies calculated in the constant-μVT ensemble and the corresponding experimental results. The interaction energy values, resulting from simulations at constant density, showed discrepancies at larger separations, exaggerated by the logarithmic scale. We see that the shape of the experimental curve is much more closer to our data resulting from simulations in the grand canonical ensemble. This indicates that this statistical ensemble combined with the DPD model is the more appropriate for studying polymer brushes under compression.

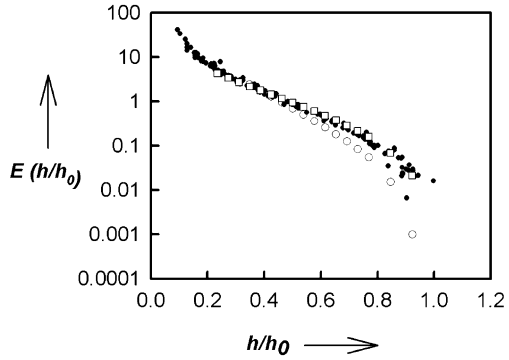

Figure 9. *Interaction energy per unit area* $E(h/h_0)$ *profiles calculated from simulations at constant* μ *(□) and constant* ρ *(○). The points (●) result from the measured forces between two grafted polystyrene brush layers onto mica surfaces in toluene.*[11]

Conclusions

We have demonstrated that the DPD model can be used in the grand canonical ensemble to simulate grafted polymer brushes under compression. In a first step, we have demonstrated from simulations of the pure DPD fluid that the simulations in the constant-μVT ensemble provide reliable values for the excess pressure and the excess chemical potential as expected from the corresponding equations of state. The use of appropriate algorithms for calculating the chemical potential in an inhomogeneous system allowed us to study grafted polymer brushes in good solvent conditions. The temperature, pressure and chemical potential profiles showed that the system in the constant-μVT ensemble is in thermal, mechanical and chemical equilibrium. We have shown that the results derived from simulations in the grand canonical ensemble are consistent with the experimental results and with the data predicted by SCF theory. More exactly, the shape of the force – distance profile calculated in the constant-μVT ensemble is close that predicted by the Alexander – de Gennes and the Milner, Witten and Cates models, assuming a flat function for the monomer density profile. The first model proposed by Milner, Witten and Cates, suggesting a parabolic profile for the brush layer, shows some discrepancies compared to the simulations at large separations.

We plan to extend this work to the study of compressed polymer brushes under shear. We recognize that the addition and removal of particles in the DPD simulation may affect the conservation laws and hence the stability of the method for simulating hydrodynamics. We will consider this point in detail in a future publication. This issue does not affect the results presented in this Article.

Computational Methods

DPD simulation model: In the DPD formalism, the individual particles are not regarded as molecules but as fluid elements. As a consequence of this coarse-graining, the conservative interactions are soft. In our model, the cutoff radius, r_c, and the particle mass, m,

were taken as unity. All other variables are given in reduced units. The particles interact through pairwise additive conservative, dissipative and random forces. The conservative force is a soft repulsion acting along the line of centres and is given by Equation (10)

$$\mathbf{f}^{\mathbf{C}}_{ij} = \begin{cases} -\dfrac{\mathrm{d}U(r_{ij})}{\mathrm{d}r_{ij}}\hat{\mathbf{r}}_{ij} = a_{ij}(1-r_{ij})\hat{\mathbf{r}}_{ij} & (r_{ij} < 1) \\ 0 & (r_{ij} \geq 1) \end{cases} \tag{10}$$

where $U(r_{ij})$ is the potential that gives rise to the conservative force $\mathbf{f}^{\mathbf{C}}_{ij}$, a_{ij} is the maximum repulsion between particles i and j, r_{ij} is the relative displacement of particles i and j and $\hat{\mathbf{r}}_{ij}$ is the corresponding unit vector. The dissipative force, $\mathbf{f}^{\mathbf{D}}_{ij}$, and the random force, $\mathbf{f}^{\mathbf{R}}_{ij}$, are given by Equations (11) and (12), respectively

$$\mathbf{f}^{\mathbf{D}}_{ij} = -\gamma w_{\mathrm{D}}(r_{ij})(\hat{\mathbf{r}}_{ij}\cdot\mathbf{v}_{ij})\hat{\mathbf{r}}_{ij} \tag{11}$$

$$\mathbf{f}^{\mathbf{R}}_{ij} = \sigma w_{\mathrm{R}}(r_{ij})\zeta_{ij}\hat{\mathbf{r}}_{ij}(\delta t)^{-1/2} \tag{12}$$

where δt is the time step, $\mathbf{v}_{ij}$ is the relative velocity of a pair of particles. w_{D} and w_{R} are the dimensionless weighting functions, σ and γ are constants. ζ_{ij} is a random Gaussian variable whose mean is 0 and which has unit variance. Espanol and Warren[19] have shown that the system has a correct equilibrium distribution in the canonical ensemble, if the following conditions, Equations (13) and (14), are satisfied,

$$w_{\mathrm{D}}(r_{ij}) = w_{\mathrm{R}}(r_{ij})^2,\ \sigma^2 = 2kT\gamma \tag{13}$$

$$w_{\mathrm{D}}(r_{ij}) = \begin{cases} (1-r_{ij})^2 & (r_{ij}<1) \\ 0 & (r_{ij} \geq 1) \end{cases} \tag{14}$$

The DPD method conserves momentum and consequently gives a correct description of hydrodynamics. In comparison, the Brownian dynamics technique does not obey Newton's third law and is a purely diffusive method. To make a grafted homopolymer chain, DPD particles are connected in linear chains using a conservative spring force. A similar harmonic force is used to model the interactions between the surface particles and their initial lattice sites.[1, 2] The equations of motion are integrated using a modified version of the velocity Verlet algorithm.

Calculation of the chemical potential: The full chemical potential μ in a spatially homogeneous system can be calculated[20] using Equation (15)

$$\mu = kT\ln\rho + kT\ln\Lambda^3 - kT\ln\left[\left\langle\exp\left(-\frac{\Delta U^{\mathrm{test}}}{kT}\right)\right\rangle_{NVT}\right] \tag{15}$$

where k is Boltzmann's constant, T is the temperature, Λ is the thermal de Broglie wavelength, ρ is the density number of the system and ΔU^{test} is the interaction energy of the test particle with the other N particles in the fluid. The first two terms represent the ideal gas chemical potential μ_{id} and the third term defines the excess chemical potential of the system. The angular brackets represent the average in the canonical ensemble. For a system with an inhomogeneity in density in the z direction, the full chemical potential $\mu(z)$ depends on the z position, according to Equation (16)

$$\mu(z) = kT\ln\Lambda^3 + kT\ln\left[\frac{\langle\rho(z)\rangle_{\mathrm{NVT}}}{\left\langle\exp\left(-\dfrac{\Delta U^{\mathrm{test}}}{kT}\right)\right\rangle_{NVT}}\right] =$$

$$kT\ln\Lambda^3 + kT\ln\langle Z(z)\rangle_{NVT} \tag{16}$$

where $\rho(z)$ and $Z(z)$ are the number density and the local activity at z, respectively. The term $kT\ln\langle Z(z)\rangle_{NVT}$ is defined by Widom[21] as the configurational chemical potential at z, $\mu^{\mathrm{conf}}(z)$. By defining the chemical potential in this way, others have shown[21–23] the constancy of the chemical potentials $\mu(z)$ and $\mu^{\mathrm{conf}}(z)$ along the z direction in the case of a nonuniform density profile $\rho(z)$.

DPD simulation in the grand canonical ensemble: The uniformity in the z direction of the full chemical potential and the local activity means that it is possible to deduce in our inhomogeneous simulations values of $\mu(z)$ and $Z(z)$ at all z, called $\langle\mu\rangle_z$ and $\langle Z\rangle_z$, respectively. In the constant-μVT ensemble, the partition function for a system of N particles possessing only translational degrees of freedom is given by Equation (17)

$$Q(\mu,V,T) = \frac{V^N\exp(\mu N/kT)}{\Lambda^{3N}N!}\int_{V^N} dr^N\exp\left[-\frac{U(r^N)}{kT}\right] \tag{17}$$

where the integration extends over the N dimensional hypervolume V^N in configurational space. In this ensemble, the number of particles can fluctuate. During the course of a normal DPD simulation, we could make a number of trial deletions and inclusions of solvent particles with equal probability. After further simplification and replacing μ by $\langle\mu\rangle_z$ in Equation (17), we find the transition probabilities for the creation or destruction of a solvent particle. The acceptance probabilities for a trial creation and deletion of a solvent particle become Equations (18) and (19)

$$P^{\mathrm{acc}}_{\mathrm{creation}} = \min\left[1, \frac{\langle Z\rangle_z \mathrm{V}}{N+1}\exp\left(-\frac{\Delta U}{kT}\right)\right] \tag{18}$$

$$P^{\mathrm{acc}}_{\mathrm{deletion}} = \min\left[1, \frac{N}{\langle Z\rangle_z \mathrm{V}}\exp\left(-\frac{\Delta U}{kT}\right)\right] \tag{19}$$

where V is the total volume of the box, T is the instantaneous temperature calculated from the kinetic energy and N is the total number of particles before the move. ΔU is the energy between the added or removed particle and the N or $N-1$ remaining particles, calculated using the conservative potential. When a creation attempt is accepted, the velocity of the corresponding particle is chosen from a Gaussian distribution with zero mean and $\sqrt{kT}$ variance. When a deletion attempted is successful the solvent particle is removed.

Simulation details: The parameter σ was chosen so that $\sigma/\sqrt{(\delta t)} = 7.07$ with a time step equal to 0.02. The reduced temperature was fixed at $kT = 2.0$. A conventional DPD simulation in the canonical ensemble was performed in a run consisting of an equilibration phase of 500 000 steps, followed by a production phase of 500 000 steps. For a DPD simulation in the constant-μVT ensemble, we used an additional step which consisted of removing a randomly chosen solvent particle or creating a new solvent particle at a randomly chosen point in the box with equal probability. The trial creation or destruction was accepted with a probability given by Equations (18) or (19), respectively. We attempted about 5000 creations and 5000 destructions in a given run; the percentage of successful attempts was between 15% and 25%, depending on the extent of the compression.

For a better efficiency in the calculation of the forces, we used the linked-cell method.[24] This method consists of partitioning the simulation box into smaller cells, each of them with dimensions slightly larger than the reduced cutoff. With this algorithm, the interactions between a given particle and its neighbours can be calculated by considering the particles that are in its same cell or in the twenty-six other linked cells surrounding it.

Acknowledgements

F.G. and P.M. are grateful to Unilever Research for its financial support for building a PC cluster with which the simulations were carried out.

Keywords: compression · computer chemistry · grand canonical ensemble · polymers

[1] P. Malfreyt, D. J. Tildesley, *Langmuir* **2000**, *16*, 4732 – 4740.
[2] D. Irfachsyad, D. J. Tildesley, P. Malfreyt, *Phys. Chem. Chem. Phys.* **2002**, *4*, 3008 – 3015.
[3] S. Alexander, *J. Phys. (Paris)* **1977**, *38*, 983 – 987.
[4] P. G. de Gennes, *Macromolecules* **1980**, *13*, 1069 – 1075.
[5] P. G. de Gennes, *Adv. Colloid Interface Sci.* **1987**, *27*, 189 – 209.
[6] S. T. Milner, T. A. Witten, M. E. Cates, *Macromolecules* **1988**, *21*, 2610 – 2619.
[7] S. T. Milner, *Science* **1991** *251*, 905 – 914.
[8] M. Murat, G. S. Grest, *Phys. Rev. Lett.* **1989**, *63*, 1074 – 1077.
[9] R. Dickman, P. E. Anderson, *J. Chem. Phys.* **1993**, *99*, 3112 – 3118.
[10] H. J. Taunton, C. Toprackcioglu, J. Klein, *Macromolecules* **1988**, *21*, 3336 – 3338.
[11] H. J. Taunton, C. Toprackcioglu, L. J. Fetters, J. Klein, *Macromolecules* **1990**, *23*, 571 – 580.
[12] T. W. Kelley, P. A. Schorr, K. D. Johnson, M. Tirrell, C. D. Frisbie, *Macromolecules* **1998**, *31*, 4297 – 4300.
[13] R. D. Groot, P. B. Warren, *J. Chem. Phys.* **1997**, *107*, 4423 – 4435.
[14] J. P. R. B Walton, D. J. Tildesley, J. S. Rowlinson, *Mol. Phys.* **1983**, *48*, 1357 – 1368.
[15] J. P. R. B Walton, D. J. Tildesley, J. S. Rowlinson, *Mol. Phys.* **1986**, *58*, 1013.
[16] B. D. Todd, P. J. Daivis, D. J. Evans, *Phys. Rev. E* **1995**, *51*, 4362 – 4368.
[17] B. D. Todd, P. J. Daivis, D. J. Evans, *Phys. Rev. E* **1995**, *51*, 1627 – 1638.
[18] D. H. Tsai, *J. Chem. Phys.* **1979**, *70*, 1375 – 1382.
[19] P. Espanol, P. B. Warren, *Europhys. Lett.* **1995**, *30*, 191 – 196.
[20] B. Widom, *J. Chem. Phys.* **1963**, *39*, 2808 – 2812.
[21] B. Widom, *J. Stat. Phys.* **1978**, *19*, 563 – 573.
[22] J. G. Powles, S. E. Baker, W. A. B. Evans, *J. Chem. Phys.* **1994**, *101*, 4098 – 4102.
[23] J. G. Powles, B. Holtz, W. A. B. Evans, *J. Chem. Phys.* **1994**, *101*, 7804 – 7810.
[24] M. P. Allen, D. J. Tildesley, *Computer Simulation of Liquids*, Clarendon, Oxford, **1987**, p. 149.

Received: July 8, 2003 [F 901]
Revised: December 15, 2003

